Research Article | Vol. 8, No. 10 | 1 Oct 2018 | OPTICAL MATERIALS EXPRESS 3049
Optical Materials EXPRESS

Single-layer active-passive Al_2O_3 photonic integration platform

CARLIJN I. VAN EMMERIK,* MEINDERT DIJKSTRA, MICHIEL DE GOEDE, LANTIAN CHANG, JINFENG MU, AND SONIA M. GARCIA-BLANCO

Optical Sciences Group, MESA + Institute for Nanotechnology, University of Twente, P.O. Box 217, 7500 AE Enschede, The Netherlands
**c.i.vanemmerik@utwente.nl*

Abstract: Amorphous Al_2O_3 is an attractive platform for integrated photonics, providing active and passive functionalities. We have developed an integration procedure to create active and passive regions at the same level on one wafer. This fabrication process reduces the number of fabrication steps compared to vertical integration of two materials. The main advantage is that all structures are defined within a single photolithography and etching step and are therefore automatically aligned. As a proof of principle, we demonstrated the luminescence of an active ring resonator with passive bus waveguide.

OCIS codes: (130.0130) Integrated optics; (130.3130) Integrated optics materials; (130.2755) Glass waveguides; (160.5690) Rare-earth-doped materials; (220.0220) Optical design and fabrication; (220.5450) Polishing.

References and links

1. P. G. Kik and A. Polman, "Erbium-doped optical-waveguide amplifiers on silicon," MRS Bull. **23**(04), 48–54 (1998).
2. P. Xing, G. F. R. Chen, X. Zhao, D. K. T. Ng, M. C. Tan, and D. T. H. Tan, "Silicon rich nitride ring resonators for rare - earth doped telecommunications-band amplifiers pumped at the O-band," Sci. Rep. **7**(1), 9101 (2017).
3. L. Agazzi, K. Wörhoff, and M. Pollnau, "Energy-transfer-upconversion models, their applicability and breakdown in the presence of spectroscopically distinct ion classes: a case study in amorphous $Al_2O_3:Er^{3+}$," J. Phys. Chem. C **117**(13), 6759–6776 (2013).
4. S. A. Vázquez-Córdova, M. Dijkstra, E. H. Bernhardi, F. Ay, K. Wörhoff, J. L. Herek, S. M. García-Blanco, and M. Pollnau, "Erbium-doped spiral amplifiers with 20 dB of net gain on silicon," Opt. Express **22**(21), 25993–26004 (2014).
5. K. Wörhoff, J. D. B. Bradley, F. Ay, D. Geskus, T. P. Blauwendraat, and M. Pollnau, "Reliable low-cost fabrication of low-loss $Al_2O_3:Er^{3+}$ waveguides with 5.4-dB optical gain," IEEE J. Quantum Electron. **45**(5), 454–461 (2009).
6. M. Demirtas, C. Odaci, N. K. Perkgoz, C. Sevik, and F. Ay, "Low loss atomic layer deposited Al_2O_3 waveguides for applications in on-chip optical amplifiers," IEEE J. Sel. Top. Quantum Electron. **24**(4), 1–8 (2018).
7. T. Ishizaka and Y. Kurokawa, "Optical properties of rare-earth ion (Gd^{3+}, Ho^{3+}, Pr^{3+}, Sm^{3+}, Dy^{3+} and Tm^{3+}) - doped alumina films prepared by the sol–gel method," J. Lumin. **92**(1–2), 57–63 (2000).
8. J. Yang, K. van Dalfsen, K. Wörhoff, F. Ay, and M. Pollnau, "High-gain $Al_2O_3:Nd^{3+}$ channel waveguide amplifiers at 880 nm, 1060 nm, and 1330 nm," Appl. Phys. B **101**(1–2), 119–127 (2010).
9. N. Purnawirman, N. Li, E. S. Magden, G. Singh, N. Singh, A. Baldycheva, E. S. Hosseini, J. Sun, M. Moresco, T. N. Adam, G. Leake, D. Coolbaugh, J. D. B. Bradley, and M. R. Watts, "Ultra-narrow-linewidth $Al_2O_3:Er^{3+}$ lasers with a wavelength-insensitive waveguide design on a wafer-scale silicon nitride platform," Opt. Express **25**(12), 13705–13713 (2017).
10. J. D. B. Bradley, L. Agazzi, D. Geskus, F. Ay, K. Wörhoff, and M. Pollnau, "Gain bandwidth of 80 nm and 2 dB/cm peak gain in $Al_2O_3:Er^{3+}$ optical amplifiers on silicon," J. Opt. Soc. Am. B **27**(2), 187 (2010).
11. G. Singh, P. Purnawirman, J. D. B. Bradley, N. Li, E. S. Magden, M. Moresco, T. N. Adam, G. Leake, D. Coolbaugh, and M. R. Watts, "Resonant pumped erbium-doped waveguide lasers using distributed Bragg reflector cavities," Opt. Lett. **41**(6), 1189–1192 (2016).
12. J. Rönn, L. Karvonen, C. Kauppinen, A. P. Perros, N. Peyghambarian, H. Lipsanen, A. Säynätjoki, and Z. Sun, "Atomic layer engineering of Er-ion distribution in highly doped $Er:Al_2O_3$ for photoluminescence enhancement," ACS Photonics **3**(11), 2040–2048 (2016).
13. M. Belt and D. J. Blumenthal, "High temperature operation of an integrated erbium- doped DBR laser on an ultra-low-loss Si3N4 platform," *Optical Fiber Communication Conference*, OSA Technical Digest (online) (Optical Society of America, 2015), paper Tu2C.7.
14. L. Agazzi, J. D. B. Bradley, M. Dijkstra, F. Ay, G. Roelkens, R. Baets, K. Wörhoff, and M. Pollnau, "Monolithic integration of erbium-doped amplifiers with silicon-on-insulator waveguides," Opt. Express **18**(26), 27703–

#340172 https://doi.org/10.1364/OME.8.003049
Journal © 2018 Received 19 Jul 2018; revised 30 Aug 2018; accepted 2 Sep 2018; published 10 Sep 2018

Optical Materials EXPRESS

27711 (2010).
15. J. Mu, M. Dijkstra, Y.-S. Yong, F. B. Segerink, K. Wörhoff, M. Hoekman, A. Leinse, and S. M. García-Blanco, "Low-loss, broadband and high fabrication tolerant vertically tapered optical couplers for monolithic integration of Si_3N_4 and polymer waveguides," Opt. Lett. **42**(19), 3812–3815 (2017).
16. Z. Su, N. Li, H. C. Frankis, E. S. Magden, T. N. Adam, G. Leake, D. Coolbaugh, J. D. B. Bradley, and M. R. Watts, "High-Q-factor Al_2O_3 micro-trench cavities integrated with silicon nitride waveguides on silicon," Opt. Express **26**(9), 11161–11170 (2018).
17. J. P. Epping, M. Hoekman, R. Mateman, A. Leinse, R. G. Heideman, A. van Rees, P. J. M. van der Slot, C. J. Lee, and K.-J. Boller, "High confinement, high yield Si_3N_4 waveguides for nonlinear optical applications," Opt. Express **23**(2), 642–648 (2015).
18. M. H. P. Pfeiffer, A. Kordts, V. Brasch, M. Zervas, M. Geiselmann, J. D. Jost, and T. J. Kippenberg, "Photonic Damascene process for integrated high-Q microresonator based nonlinear photonics," Optica **3**(1), 20 (2016).
19. S. Yew, T. Liu, M. Lur, and W. Sun, "Dual damascene process," U.S. patent US5801094A (September 1, 1998).
20. S. Deleonibus and B. Guillaumot, "Damascene architecture electronic storage and method for making same," U.S. patent US6955963B2 (2005).
21. P. Loiko, N. Ismail, J. D. B. Bradley, M. Götelid, and M. Pollnau, "Refractive-index variation with rare-earth incorporation in amorphous Al_2O_3 thin films," J. Non-Cryst. Solids **476**, 95–99 (2017).
22. Y. Fan, R. M. Oldenbeuving, C. G. Roeloffzen, M. Hoekman, D. Geskus, R. G. Heideman, and K.-J. Boller, "290 Hz Intrinsic Linewidth from an Integrated Optical Chip-based Widely Tunable InP-Si_3N_4 Hybrid Laser," in *Conference on Lasers and Electro-Optics* (OSA, 2017), p. JTh5C.9.
23. N. Li, D. Vermeulen, Z. Su, E. S. Magden, M. Xin, N. Singh, A. Ruocco, J. Notaros, C. V. Poulton, E. Timurdogan, C. Baiocco, and M. R. Watts, "Monolithically integrated erbium-doped tunable laser on a CMOS-compatible silicon photonics platform," Opt. Express **26**(13), 16200–16211 (2018).
24. D. T. Spencer, T. Drake, T. C. Briles, J. Stone, L. C. Sinclair, C. Fredrick, Q. Li, D. Westly, B. R. Ilic, A. Bluestone, N. Volet, T. Komljenovic, L. Chang, S. H. Lee, D. Y. Oh, M.-G. Suh, K. Y. Yang, M. H. P. Pfeiffer, T. J. Kippenberg, E. Norberg, L. Theogarajan, K. Vahala, N. R. Newbury, K. Srinivasan, J. E. Bowers, S. A. Diddams, and S. B. Papp, "An optical-frequency synthesizer using integrated photonics," Nature **557**(7703), 81–85 (2018).
25. J. D. B. Bradley, F. Ay, K. Wörhoff, and M. Pollnau, "Fabrication of low-loss channel waveguides in Al_2O_3 and Y_2O_3 layers by inductively coupled plasma reactive ion etching," Appl. Phys. B **89**(2–3), 311–318 (2007).
26. K. Wefers and C. Misra, *Oxides and Hydroxides of Aluminum* (1987), **19**.
27. E. Nakazawa and S. Shionoya, "Cooperative Luminescence in $YbPO_4$," Phys. Rev. Lett. **25**(25), 1710–1712 (1970).

1. Introduction

Amorphous Al_2O_3 is an attractive material for integrated photonics, providing active and passive functionalities when doped with rare-earth ions. Whereas Si and Si_3N_4 have a low solubility for rare-earth ions [1,2], amorphous Al_2O_3 can host high concentrations of those ions with moderate quenching of luminescence [3,4]. The ability to host high concentrations of rare-earth ions in combination with the wide transparency window (150-7000 nm) and low propagation loss [5,6], makes amorphous Al_2O_3 an attractive material for UV, visible, near- and mid-IR on-chip active devices [7–9].

Many different lasers and amplifiers have been demonstrated in the last few years using amorphous rare-earth ion doped Al_2O_3 as gain material [4,10–12], as well as rare-earth ion doped Al_2O_3 in combination with passive photonic platforms, such as Si_3N_4 [13–15]. The realization of the active devices in a fully doped Al_2O_3 layer has two main limitations, namely a restriction in the dopant concentration that can be used and lack of integration with other optical functions on the chip. The current integration schemes rely on several photolithography steps, which introduce losses due to misalignment [15,16].

In this work, we propose a single-layer monolithic integration scheme to integrate active and passive regions on a wafer. The proposed method is based on a photonics damascene method [17,18], derived from the process used in microelectronics [19,20]. Using this approach, only one lithography and etching step is required to fabricate all functionalities, leading to self-aligned transitions from the passive to the active sections. Since the difference of refractive index between doped and undoped Al_2O_3 is minimal [21], very low transition losses are expected. Furthermore, the low loss of the undoped Al_2O_3 waveguide will permit the realization of complex integrated photonic devices [22–24].

Optical Materials EXPRESS

In this work, the fabrication process developed for the realization of the one-layer active-passive wafer is detailed. As a proof of principle, an active ring resonator coupled to a passive bus waveguide is experimentally demonstrated.

2. Fabrication process of one-layer active-passive Al_2O_3

In this work we want to demonstrate the integration of Yb^{3+}-doped ring resonators with passive bus waveguides. The fabrication flow is shown schematically in Fig. 1. Firstly, active regions of Yb^{3+}:Al_2O_3 (650 µm wide and 1000-3550 µm long) are deposited by RF reactive co-sputtering (process described in the next section) with a target height of ~400 nm through a shadow mask. This thickness guarantees single mode operation at the pump and signal wavelengths (λ_{pump} = 976 nm, λ_{signal} ≈1030 nm) in a ring resonator with a waveguide cross-section of 1.8 x 0.4 µm^2 and a radius of 200 µm. Those regions are then overgrown with a roughly 200 nm thicker passive layer (i.e., ~600 nm undoped Al_2O_3). A chemical mechanical planarization (CMP) step is performed to planarize the active-passive layer, producing a wafer with a planar layer of undoped Al_2O_3 with regions of active rare-earth ion doped material in it. Waveguides are then fabricated using standard lithography and inductively coupled reactive ion etching (Oxford Plasma Pro 100 Cobra) with BCl_3/HBr gases optimized for Al_2O_3 etching [25]. Finally the waveguides are protected with a thick oxide layer deposited by plasma enhanced chemical vapor deposition (PECVD) as cladding.

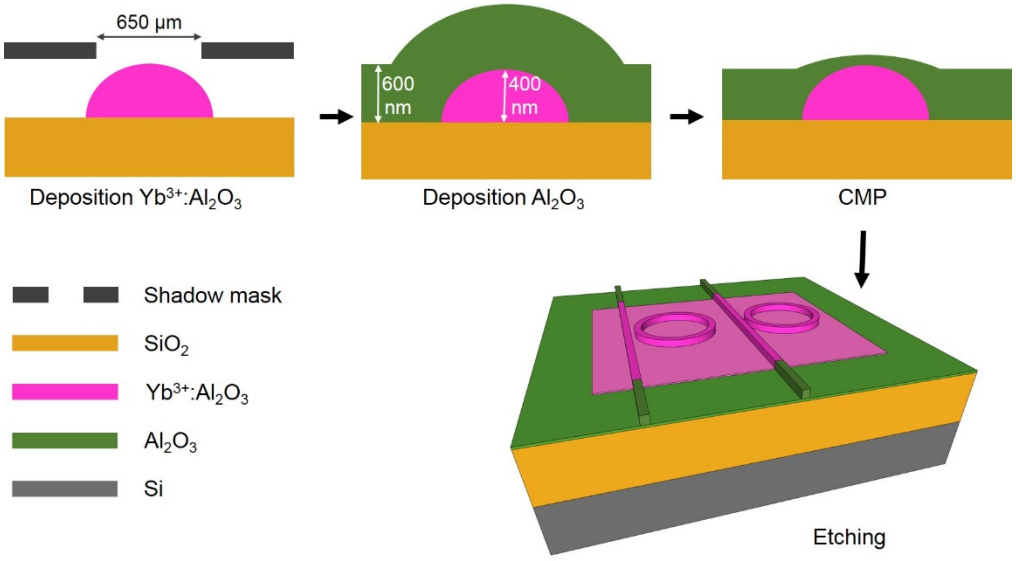

Fig. 1. Schematic representation of the fabrication process of active-passive Al_2O_3 devices, showing consecutively the deposition of Yb^{3+}:Al_2O_3 through a shadow mask (target thickness of 400 nm), the deposition of the undoped Al_2O_3 layer (target thickness of 600 nm), planarization using CMP and waveguide fabrication by etching.

2.1 Reactive co-sputtering of Al_2O_3

The Al_2O_3 layers are deposited by radio-frequency (RF) reactive co-sputtering using an AJA ATC 1500 instrument [5]. Argon flows of 25 and 5 sccm are applied to respectively the aluminum (Al, 99.9995% purity) and ytterbium (Yb, 99.9% purity) metallic targets and an oxygen flow of 4 sccm is added to the process to ensure full oxidation of the layer. When depositing an undoped layer, a RF sputtering power of 200 W was applied to the Al-target and an additional RF sputtering power of 20 W was applied on the Yb-target when depositing the active regions. The reaction chamber was pre-evacuated to 0.2 mTorr to reduce the OH^- level, whereas the pressure was kept around 4 mTorr during the deposition process. OH^- free

Optical Materials EXPRESS

deposition is required for devices based on rare-earth ion transitions, because these bonds induce strong luminescence quenching and therefore, greatly diminish or hinder optical gain. The wafer is positioned 17 cm from the target and is heated to 650 °C, to ensure the deposition of uniform dense layers.

The active regions are deposited through a shadow mask. This mask is made from 200 µm thick 301 stainless steel. The openings for the deposition of active regions are made by laser cutting (Rofin MPS). All regions have a width of 650 µm and lengths varying from 1000 to 3550 µm. Those areas are made such that a consecutive row of 5 similar rings, with a radius ranging from 50 to 300 µm, are covered, as shown in Fig. 2(a). The openings are placed in a line of six (for the 6 different ring radii) and the structure is repeated homogeneously over the wafer to ensure equal planarization.

First the shadow mask is aligned with the wafer flat and clamped together in the holder. Then the deposition is done as described in the previous paragraph. The deposition rate of the active regions through the shadow mask openings is roughly 75% of the normal deposition rate and the regions have a curved profile, as shown in Fig. 2(b). Both features are caused by the shielding effect of the shadow mask. There are three targets available for deposition (Al, Er, Yb), which are present in the reaction chamber under an angle, such that they all point in a similar way to the wafer. The sides of the open regions in the mask are 200 µm high and therefore a part of the exposed region on the wafer is shielded from the plasma. To minimize this feature the wafer is rotating. There is also a small gap between the mask and wafer and due to the angle of incidence of the plasma, Al_2O_3 particles can deposit slightly underneath the mask, as shown in Fig. 2(c). The influence of the mask, for the opening width of 650 µm, is too big to achieve an uniform top layer in the deposited regions. The width of the regions should at least be doubled to obtain a plateau region of a couple of tens of micrometers in the deposited regions.

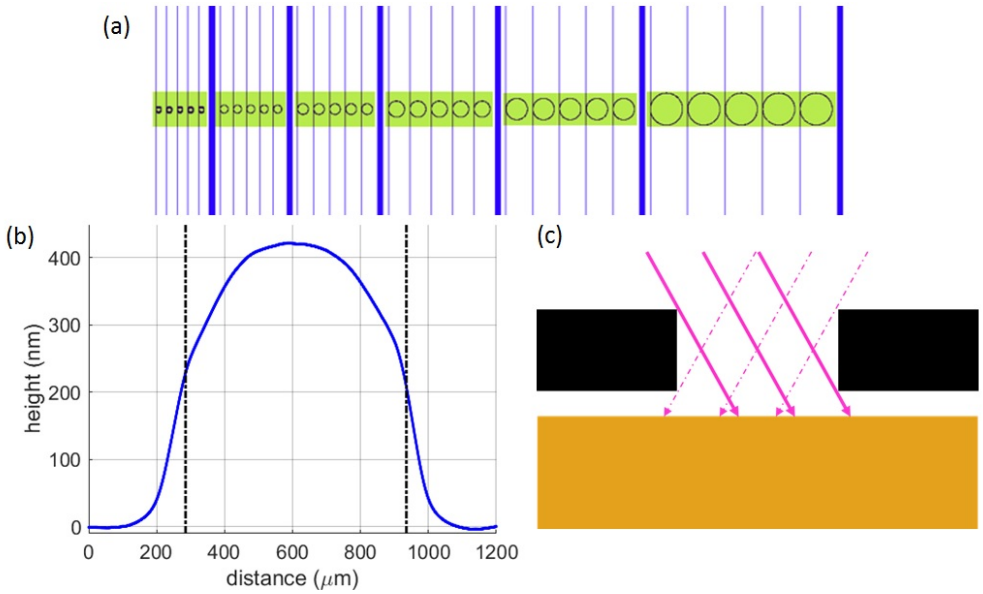

Fig. 2. (a) Representation of the chip layout with waveguides and ring resonators (blue) and active regions (green). (b) Profile scan along the width of a deposited Yb^{3+}:Al_2O_3 region, the dashed vertical lines represent the sidewall of the shadow mask. (c) Schematic representation of the deposition of Yb^{3+}:Al_2O_3 (pink arrows) with a shadow mask (black) on SiO_2 (yellow). Continuous and dashed pink arrows represent the direction of the plasma during deposition.

Optical Materials EXPRESS

2.2 Chemical mechanical planarization of Al_2O_3

A wafer with active regions has been fabricated with the above mentioned procedure. This resulted in an active region with a maximum height of 290 nm (target was 400 nm). The height is lower than expected due to the lower deposition rate caused by the influence of the mask. The active regions were overgrown with a 480 nm thick undoped Al_2O_3 to complete the layer, as shown in Fig. 3(a).

After fabrication of the layer, there is a 290 nm high bump on top of the layer, as shown in Fig. 3(a). This has to be planarized to enhance the quality of the lithography and etching process and to achieve the right waveguide dimensions. Therefore a chemical mechanical planarization (CMP) process was developed, using a Mecapol E460 CMP machine in combination with an IC1000 pad from DOW.

The main planarization was done using a solution of Semi Sperse 25 (SS25) slurry diluted in a ratio of 1 to 2 with DI water. The pH was adjusted with 2% HCl solution to 7, in order to obtain a more mechanical driven removal [26]. During the first CMP step of 60 seconds the focus was to planarize the wafer, mainly reducing the height of the bumps. To ensure this, only the bumps had to be in contact with the pad and therefore a pressure of 0.50 bar was used on the wafer. To have a high removal rate the rotation speed of the table and head was set to 70 rpm. The focus for the second step of 60 seconds was to achieve the correct layer thickness and have further planarization. Therefore the pressure on the wafer was increased to 0.75 bar to ensure that the whole wafer was in contact with the pad. The rotation speed of the table and head was set to 50 rpm for a removal rate of ~50 nm/min for the main surface of the wafer. For the final smoothening step, a slurry with a ratio of 1 to 2, SS25 to DI water with a pH of 8 was used, to have a chemical dominated removal. The same settings as in the second step were used for 120 seconds because the removal rate was much lower.

The final layer is shown in Fib. 3(b), where the layer of passive Al_2O_3 is 400 nm and there is still a bump of 120 nm on top of this layer. This is not beneficial for optimal performance of the waveguides because there will be a smaller optical overlap with the active region. Further optimization of the deposition through a shadow mask and planarization of the wafer is underway.

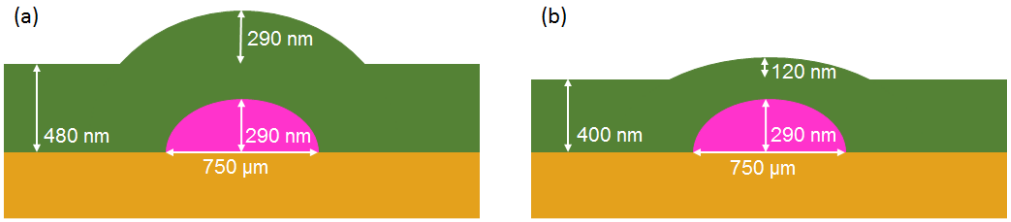

Fig. 3. Schematic representation of the layer thicknesses of active, passive and bump (a) after deposition; (b) layer thicknesses after CMP. The height and width of a bump and the thickness of the undoped layer were measured in a central position of the wafer with respectively a profilometer (Veeco Dektak 150) and ellipsometer (Woollam M-2000UI).

3. Demonstration of one-layer active-passive Al_2O_3

Ring resonators with an input-output bus waveguide where fabricated with the fabrication procedure described above. The active layer (Yb^{3+}:Al_2O_3) thickness in this sample was 290 nm with an overall final layer thickness of 400 nm (Fig. 3(b)). Light was butt coupled into the input bus waveguide through a polarization maintaining fiber. To enhance the coupling efficiency to the chip index matching fluid was utilized. The device was pumped at 976 nm to excite the Yb^{3+} ions in the doped region. A photo of the luminescence in the active region was taken with a standard photo camera through a microscope objective such that the rings of a couple of tens of micrometers are clearly visible, as shown in Fig. 4. The luminescence is in the visible regime is probably due to Er^{3+} or Tm^{3+} impurities in the active region. At the top

Optical Materials EXPRESS

of the ring a weaker, tilted, straight line is visible. This is caused by stray light from the in-coupling light, which luminesces in the active region. The dopant concentration utilized was too low, which, in combination with the relatively low overlap with the pump (i.e., 290 nm thick doped layer in a 400 nm total thickness of Al_2O_3, comparable with 43% of the power in the fundamental mode overlapping the active region) prevented lasing from the device. In Fig. 4, a taper transition region is visible at both ends of the active part of the bus waveguide. Due to the deposition with the shadow mask, a vertical taper is naturally formed between the passive and active Al_2O_3 regions, which leads to an adiabatic transition. Since the fabrication is realized in a single lithography and etching step, no misalignment in that region occurs, further increasing the efficiency of the transition. Towards the center of the active region the fraction of doped layer slightly increases and therefore the luminescence becomes stronger.

This result is the first demonstration of the integration in a single photonic layer of active and passive dielectric materials. It paves the road towards on-chip lasers and amplifiers that can directly be integrated with passive building blocks on the same platform minimizing the need for accurate alignment procedures.

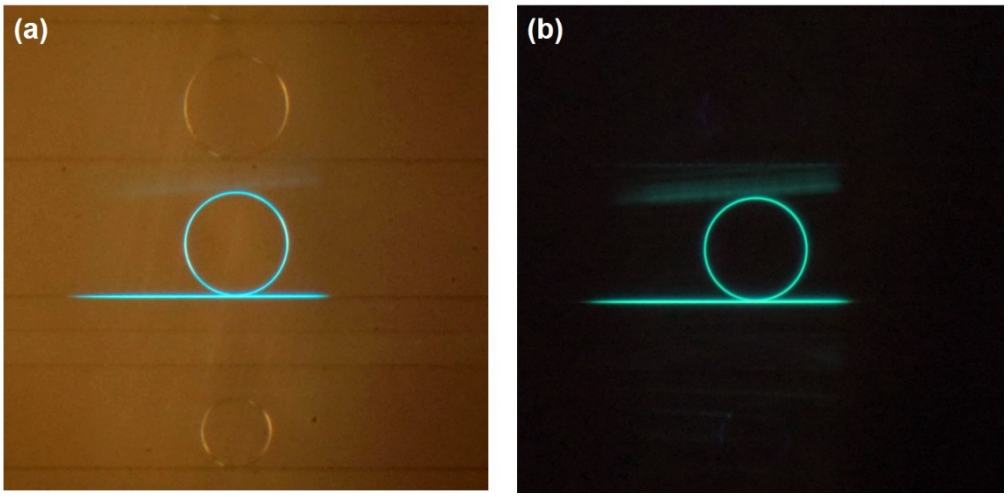

Fig. 4. Photograph of (a) Chip containing rings with a radius of 100 and 150 µm showing the luminescence of the ytterbium doped active region in the center ring. (b) Same photograph without background light. Luminescent stray light can be observed on the top of the ring.

4. Conclusion

This work represents the first one-layer active-passive Al_2O_3 integration. The fabrication procedure for the layer is explained in detail and a preliminary device demonstration is shown. The working principle have been experimentally demonstrated by the luminance of Yb^{3+} ions only in the active region.

Funding

European Research Council Consolidator Grant (ERC) (grant project RENOS "Rare-earth doped novel on-chip sources"- 648978)